ELSEVIER

Contents lists available at ScienceDirect

International Journal of Biological Macromolecules

journal homepage: www.elsevier.com/locate/ijbiomac





Fluorescent HIV-1 integrases for a suite of new user-friendly stability, nucleic acid binding and strand transfer activity assays

Rebecca A. Bourquin, Alanna E. Sorenson, Patrick M. Schaeffer

Biomedical Sciences and Molecular Biology, College of Medicine and Dentistry, James Cook University, Douglas, QLD 4811, Australia

ARTICLE INFO

Keywords: HIV-1 Integrase activity mCherry GFP DNA binding qPCR Thermal stability assay

ABSTRACT

Human immunodeficiency virus (HIV) infects CD4+ T-cells, causing acquired immunodeficiency syndrome. Despite advances in antiretroviral therapy, drug resistance remains a critical issue. HIV integrase is a key therapeutic target. Resistance to integrase strand transfer inhibitors requires development of new drugs with distinct mechanisms. Integrases tethered with GFP (IN-GFP) and mCherry (IN-mCherry) were evaluated for the development of a comprehensive suite of user-friendly assays. A new fluorescent protein-based stability assay (FP-Basta) effectively assessed protein thermal stability, revealing aggregation midpoints of 45.0 °C for IN-GFP and 45.4 °C for IN-mCherry. FP-Basta showed that IN-mCherry was stabilized by a target DNA and viral LTR, confirming protein-DNA interactions. A new qPCR-based integrase activity assay demonstrated robust detection of strand transfer activity, with a ~21,500-fold sensitivity over background. Manganese ions were essential, enhancing integrase activity assay can distinguish 3′-processing and strand transfer activities and was validated for inhibitor screening. The combination of FP-Basta and qPCR-based integrase activity assay provides a comprehensive, cost-effective platform for evaluating IN function and inhibitor efficacy. These tools, leveraging GFP- and mCherry-tagged IN, offer potential for future high-throughput applications in HIV drug discovery and the development of therapies addressing resistance challenges.

1. Introduction

Human immunodeficiency virus (HIV) targets the CD4 $^+$ T-cells of the human immune system and as a result, causes immunodeficiency (AIDS) in infected individuals. Globally, an estimated 37.7 million [30.2–45.1 million] people were living with HIV/AIDS at the end of 2020 and in that year alone, 680,000 [480,000–1.0 million] deaths were attributed to HIV/AIDS and its associated conditions [1]. However, the number of AIDS-related deaths globally has decreased by 47 % between 2010 and 2020 and the number of yearly new infections has decreased by 31 % – thanks to a positive increase in antiretroviral therapy (ART) coverage from 25 % to 73 % globally [2].

The HIV integrase (IN) is an essential protein involved in viral replication making it an ideal drug target [3–5]. The HIV IN is a 32 kDa protein comprising 288 amino acid residues. It can be divided into 3 domains: an N-terminal domain (residues 1–50) that is involved in zinc binding and multimerization [6]; a catalytic core domain (CCD) (residues 50–212) that contains the active site of the IN protein – two divalent magnesium or manganese ions coordinated to Asp64, Asp116,

and Glu152 residues [7,8]; and a C-terminal domain (residues 212–288) that binds DNA non-specifically [9]. The IN is essential to multiple stages of the HIV-1 viral lifecycle and performs essential catalytic steps. These include 3'-processing where IN removes a GT dinucleotide from both 3' ends of the viral DNA long terminal repeats (LTR), and strand transfer where IN inserts the processed DNA into the host genome. Additional key properties of IN include dimerisation, tetramerisation, and DNA binding [10].

Targeting the essential function IN plays in strand transfer has been a very successful approach, demonstrated by the successful development of the IN strand transfer inhibitors (INSTI), raltegravir, elvitegravir, dolutegravir, bictegravir and cabotegravir, and their introduction into the general ART treatment regime for HIV-1 [3,4]. However, the efficacy of INSTI is increasingly undermined by drug resistance and crossresistance due to their similar structures and mechanisms of inhibition, which has increasingly been observed in vitro and in patients during treatment [11]. As such, the development of IN-targeting drugs with new mechanisms of action or structures may reduce occurrence of drug resistance during HIV-1 treatment and cross-resistance [12]. For

E-mail address: patrick.schaeffer@jcu.edu.au (P.M. Schaeffer).

^{*} Corresponding author.

this, new high-throughput drug screening assays capable of exploring novel modes of IN inhibition are needed.

GFP and mCherry tagged IN have previously been expressed in bacteria for protein production [13] and in eukaryotic cells for the evaluation of gene therapy and protein transduction [14]. Tethering GFP or mCherry to IN allows simple and effective monitoring of the protein's fate during expression, purification and assay development. However, GFP and mCherry are large fluorescent proteins that may sterically affect IN activity. Of note, mCherry has previously been reported to increase protein solubility [15]. The wild-type IN protein is notoriously difficult to produce due to its inherently low solubility [16]. Furthermore, even small changes in the IN amino acid sequence can result in significant differences in solubility, activity and structure [17,18]. As such, IN fusion proteins should be characterised carefully to ensure their activities are unaffected. Here we compared the stability, nucleic acid binding and enzymatic activities, of C-terminal GFP- and mCherry-tagged IN for the development and evaluation of a suite of new user-friendly assays with potential for high-throughput applications.

2. Methods

2.1. Expression of GFP- and mCherry-tagged integrase

IN-GFP and IN-mCherry vectors (pAC284 and pAC299 respectively) were created by Dr. Alanna Sorenson [13] and used in this project. IN-GFP and IN-mCherry proteins were expressed using similar methods to those previously described for IN-GFP [13]. Briefly, competent cells (E. coli KRX or E. coli BL21(DE3) RIPL) were transformed with either pAC284 or pAC299 and grown on LB agar plates containing glucose (1 % w/v) and appropriate antibiotics (KRX: ampicillin (100 µg/mL); BL21 (DE3) RIPL: ampicillin (100 $\mu g/mL$) and chloramphenicol (50 $\mu g/mL$)) overnight at 37 $^{\circ}$ C. A LB culture (5 mL) supplemented with suitable antibiotics was then inoculated with a single colony and incubated overnight at 37 °C with shaking at 250 rpm. Dependent on the bacterial strain used, this overnight culture was added to either TB medium (100 mL) containing ampicillin (100 $\mu g/mL$) for KRX, or autoinduction medium (100 mL) supplemented with ampicillin (100 $\mu g/mL$) and chloramphenicol (50 $\mu g/mL$) for BL21(DE3) RIPL, to give a final OD₆₀₀ of ${\sim}0.125.$ Cultures were incubated at 37 $^{\circ}\text{C}$ and shaken at 250 rpm until an OD600 of 1 was reached. Rhamnose (20 %) was added to a final concentration of 0.1 % w/v if the KRX strain was used, and the cultures were then incubated at 16 °C and 250 rpm for 48-72 h. Once the OD₆₀₀ reached between 10 and 15 and had ceased increasing, the culture was centrifuged for 30 min at 3838 rcf and the supernatants were discarded. The resulting cell pellets were snap frozen with liquid nitrogen and stored at $-80\,^{\circ}$ C. After completion of protein expression, a 5 μL aliquot of OD_{600} -normalised bacterial culture was combined with 5 μL of PBS on a glass slide, dried at 37 $^{\circ}$ C, and covered with a further 10 μ L of PBS and a coverslip. Slides were imaged using fluorescence microscopy at 400× magnification, with the FITC filter used for GFP fluorescence and the Texas Red filter used for mCherry fluorescence.

2.2. Purification of GFP- and mCherry-tagged integrase

Lysis and purification were performed as previously described [13]. In brief, the bacterial pellet was thawed on ice and resuspended in 7.5 mL of lysis buffer per gram of cell pellet. The cell suspension was then passed through a French pressure cell at 12000 psi for cell lysis and clarified for 30 min at 40,000 rcf at 4 °C. The supernatant was passed twice through a 1 mL bed volume of pre-equilibrated Profinity IMAC Ni-IDA resin (Bio-Rad), the resin was washed three times with 5 mL lysis buffer (Na₂HPO₄ (0.045 M), NaH₂PO₄ (0.005 M), NaCl (0.3 M), imidazole (0.01 M), 2-mercaptoethanol (2 mM) and glycerol (10 % ν/ν final)), and the protein was eluted in 4–5 fractions (1.5 mL each) with elution buffer (lysis buffer with imidazole (0.2 M)). Each fraction was then combined with an equal volume of saturated ammonium sulphate

(kept at 25 °C), mixed gently at 4 °C overnight, and centrifuged at 57590 rcf for 30 min. The supernatants were removed, and the pellets were snap frozen and stored at -80 °C. The purification yield was estimated using fluorescence measurement, and the protein concentration was measured using a Bradford assay. SDS-PAGE was used to analyse composition and purity of protein samples. Samples were not heat-treated for direct fluorescence capture (GFP-Basta).

2.3. Fluorescent protein-based stability assay

A GFP-Basta was performed as previously described [19] and was adapted for mCherry-tagged proteins. This technique will therefore be referred to as a FP-Basta. Samples (15 μ L) of pre-centrifuged IN-GFP, INmCherry and GFP (35-50 μM each) were combined and diluted in phosphate buffer (Na₂HPO₄ (0.045 M), NaH₂PO₄ (0.005 M), 2-mercaptoethanol (2 mM) and glycerol (10 % v/v final)) to a final volume of 225 $\mu L.$ Aliquots (22.5 $\mu L)$ of this mixture were taken and incubated for 10 min at nine different temperatures: 25.0 °C, 35.0 °C, 36.7 °C, 39.8 °C, 44.2 °C, 50.2 °C, 54.9 °C, 58 °C and 60.0 °C. These samples were then cooled on ice for 10 min and centrifuged for 20 min at 34840 rcf and 4 °C. Subsequently, either 7.5 μL aliquots of the supernatant were analysed using SDS-PAGE, and ImageJ was used to quantify the band intensity for each protein, or 3 µL aliquots of the supernatant were added to 47 μ L of buffer IS (HEPES pH 7.5 (25 mM), glycerol (10 % ν/ν final) and 2-mercaptoethanol (2 mM)) in a black 96-well plate, and fluorescence was measured. Measurements were normalised to the fluorescence of the 25 °C sample. Aggregation midpoint temperatures were determined with GraphPad Prism version 9.3.1 using a Boltzmann sigmoidal fit.

2.4. Isothermal FP-Basta

An isothermal FP-Basta was performed as described by Moreau et al. [19]. IN-mCherry and GFP (10 μM each final concentration) were combined with either the LTR or T1 (10 μM final) in buffer IR (HEPES pH 7.5 (25 mM), MgCl $_2$ (5 mM), MnCl $_2$ (5 mM) and 2-mercaptoethanol (2 mM)) and left at RT for 10 min to equilibrate. Half of the sample was then heated to 54.9 °C for 10 min, while the other half of the sample was left at RT as a control. All samples were then cooled rapidly on ice for 10 min, centrifuged for 20 min at 34840 rcf, and a 3 μL aliquot of each supernatant was added to 47 μL of buffer IS (HEPES pH 7.5 (25 mM), glycerol (10 % ν/ν) and 2-mercaptoethanol (2 mM)) in a black 96-well plate. Fluorescence was measured and normalised to the fluorescence of the sample kept at room temperature.

2.5. Differential scanning fluorimetry of a GFP-tagged protein

DSF-GTP reactions were performed on IN-GFP as described by Moreau et al. [20]. A sample of IN-GFP (20 $\mu L,\,20~\mu M)$ was transferred to a hard-shell 96-well PCR plate and sealed using plate sealing film. A melt curve was performed from 25 °C to 90 °C, with 0.5 °C increments every 30 s in a Bio-Rad C1000 Touch Thermal Cycler with the CFX96 Touch Real-Time PCR Detection System. GFP fluorescence was detected using the FAM channel, and the output data were analysed in GraphPad Prism version 9.3.1.

2.6. Electrophoretic mobility shift assay of fluorescent proteins

An electrophoretic mobility shift assay of a GFP-tagged protein (GFP-EMSA) [21] was utilised for both IN-GFP and IN-mCherry, and therefore will be referred to as a FP-EMSA. For non-specific DNA binding, T1 top strand and T1 bottom strand (see ESI Table 1) were annealed to form T1 (see ESI Table 2) by heating to 95 °C for 5 min and slowly cooling in buffer OA (Tris-HCl pH 8 (20 mM) and NaCl (150 mM)). LTR binding was assessed using the pre-processed LTR top strand and LTR bottom strand (see ESI Table 1) annealed as above. RNAse-treated (0.0055

Kunitz RNAse A, 1 h, 25 °C) protein suspensions (4 µL, 25 µM) were then combined with 1 µL of MgCl $_2$ solution (100 mM) and 1 µL of either T1 or pLTR DNA (7.5 µM). This mixture was then made up to a final volume of 10 µL with phosphate buffer and left at room temperature for 10 min, before 1 % agarose gel electrophoresis at 80 V for 40 min. Using a G:BOX Chemi XRQ, GFP fluorescence was imaged using blue light and the 525 filter, and mCherry fluorescence was captured using green light and the 605 M filter. The gel was stained with a 3X GelRed solution for 40 min, followed by transillumination with mid-wave UV light (302 nm) and the UV06 filter to visualise DNA bands.

2.7. Standard strand transfer IN activity assay

T1 (1.25 μ L, 0.8 μ M), LTR (1.25 μ L, 0.8 μ M) (see ESI Table 1), and 2X buffer IR (5 μ L) were combined and added to an RNAse-treated (0.0055 Kunitz RNAse A, 1 h, 25 °C) protein solution (2.5 μ L, 4 μ M) on ice. Reactions were started in a Kyratec SC200 SuperCycler thermal cycler at 37 °C for 1 h followed by 90 °C for 10 min and held at 4 °C.

Alternatively, a mixture of T1 and LTR in nuclease free water (2.5 μL , 0.8 μM each) was combined with either 2.5 μL of 4X buffer IR and 1 μL Milli-Q water, or 2.5 μL of 4X HEPES buffer (HEPES pH 7.5 (0.1 M), 2-mercaptoethanol (8 mM)) and 1 μL MnCl $_2$ solution (1 mM). A sample (1.5 $\mu L)$ of a compound, for example EDTA or DMSO, or Milli-Q water was then added to this mixture. This 7.5 μL mixture was then added to a sample of RNAse-treated (0.0055 Kunitz RNAse A, 1 h, 25 °C) protein solution (either IN-mCherry or GFP, 2.5 μL , 4 μM in buffer IS) in a PCR tube. Reactions were incubated at 37 °C for 1 h, heat inactivated at 90 °C for 10 min and held at 4 °C in a Kyratec SC200 SuperCycler thermal cycler.

2.8. qPCR

A 5 μL aliquot of 200-fold diluted reaction mixture was then combined with 10 μL of a 2X SYBR® green qpCR mix (either BioRad iTaqTM Universal SYBR® Green Supermix or Bioline SensiFAST SYBR® No-ROX) and 5 μL of appropriate primer mix (e.g. 2 μM T1 forward primer and 2 μM T1 reverse primer) in a hard-shell 96-well PCR plate and sealed using plate sealing film. Integration events were then detected by qPCR (see ESI Table 3) in a Bio-Rad C1000 Touch Thermal Cycler with the CFX96 Touch Real-Time PCR Detection System. qPCR RFU data were imported into LinRegPCR version 2020.2 for baseline correction, quality analysis, and to determine individual PCR efficiencies.

The positive control psJCU488 (see ESI Table 1) was serially diluted and amplified using the qPCR conditions (see ESI Table 3). The log of template DNA concentration was plotted against the Cq value to determine the slope. Primer efficiency was calculated using Eq. (1) below:

Percentage efficiency =
$$(10^{-1/\text{Slope}} - 1) \times 100$$
 (1)

3. Results

3.1. Protein expression and purification

IN-GFP and IN-mCherry expression was trialled in BL21(DE3) RIPL and KRX *E. coli*. IN-GFP could be expressed in both strains, however IN-mCherry appeared to affect bacterial growth in BL21(DE3) RIPL and its expression was unsuccessful. The solubility of these proteins was compared by fluorescence microscopy (ESI Fig. 1). A proportion of IN-GFP and IN-mCherry was expected to be insoluble and aggregated, as the wild-type IN sequence had been reported to have low solubility [16]. Inclusion bodies were clearly visible for IN-GFP and IN-mCherry, confirming that a large fraction of both proteins was aggregating. Slightly fewer inclusion bodies were visible in the IN-mCherry-expressing bacteria. It is unclear whether this is due to differential expression in these *E. coli* strains or whether IN-mCherry is indeed more soluble than IN-GFP

(ESI Fig. 1). Proteins were purified using a previously described cell lysis and nickel affinity chromatography workflow [13] (ESI Fig. 2). The purification of GFP and mCherry was straightforward. In contrast, IN-GFP and IN-mCherry (ESI Fig. 2A–B) purifications and quality control (ESI Fig. 2C) were problematic compounded by proteolysis of the IN and mCherry [22]. Overall, most of the fluorescent proteins were lost during the nickel affinity purification step, with final yields of only approximately 1 % for IN-GFP and IN-mCherry (see ESI Fig. 2D and extended text 1).

3.2. Protein thermal stability

DSF [23-26] has previously been used to characterise the thermal stability of IN. Transition midpoint temperature (T_m) values of 48.1 °C and 51.5 °C were reported in different buffer systems [27,28]. However, due to protein contaminations in both IN-GFP and IN-mCherry samples, the dye-based DSF method was not an option. DSF-GTP [13,20] measures changes in the fluorescence of GFP tethered to a protein of interest to determine its T_m. This eliminates the need for pure protein samples, and avoids interferences with the solvatochromic dyes used in conventional DSF. DSF-GTP with IN-GFP yielded a T_{m} value of 45.0 $^{\circ}\text{C}$ (Fig. 1A), however the IN peak was small as previously noted by Sorenson and Schaeffer [13]. Moreover, T_m values could not be determined for IN-mCherry likely due to the mCherry fluorescence properties [29]. The GFP-Basta [19] was chosen as an alternative method and adapted for mCherry fluorescence (recoined FP-Basta). Samples were heated in a 25-60 °C temperature gradient to determine the transition midpoint of aggregation (Tagg) values of IN-GFP and IN-mCherry. GFP fluorescence was unaffected in this temperature range (Fig. 1B). Using FP-Basta, near identical T_{agg} values of 45.0 °C (95 % CI: 43.05 °C to 47.36 °C) and 45.4 °C (95 % CI: 43.23 °C to 48.25 °C) were obtained for IN-GFP and INmCherry respectively. Overall, the T_{m} and T_{agg} values were similar. However, our T_m value (IN-GFP in phosphate buffer) was slightly lower than the previously reported values in HEPES [27] or MOPS [28] buffers

3.3. RNA and DNA binding

The IN binds RNA [5] which may impact the DNA binding of IN-GFP and IN-mCherry. RNA contamination was examined by FP-EMSA [21] (Fig. 2) and observed as a fluorescent smear, particularly in untreated IN-mCherry samples. RNAse A treated samples decreased the RNA smear and the mobility of IN-GFP and IN-mCherry protein suggesting the occurrence of significant protein-RNA interactions. RNA binding of IN-mCherry was further examined using a FP-Basta [19]. A significant decrease in $T_{\rm agg}$ from 52.8 °C to 46.2 °C was observed after RNAse A digestion (Fig. 2B) in buffer IS. Consequentially, IN-GFP and IN-mCherry samples were systematically treated with RNAse A to eliminate possible interference with DNA binding.

IN binds a specific sequence within the viral DNA LTR region and the host DNA non-specifically [8,10]. A DNA target (T1) with no commonly known IN binding sites and a pre-processed viral LTR DNA (pLTR) were designed (see ESI Table 2) and examined with IN-mCherry using FP-Basta. Approximately 20 % of the fluorescent protein remained soluble at 54.9 °C. Thus, isothermal FP-Basta was performed at 54.9 °C (Fig. 2C). The formation of IN-DNA complex was expected to stabilise IN, increasing the fraction of folded protein. IN-mCherry was significantly stabilized in the presence of T1 and pLTR (Fig. 2C). FP-EMSA confirmed IN-GFP and IN-mCherry binding to T1 and the LTR. A discrete protein band shift and a smeared DNA band shift was observed for both IN-GFP and IN-mCherry in the presence of T1, indicating the formation of a protein-DNA complex (see ESI Fig. 4A). Relative to the DNA control, the intensity of the T1 DNA band decreased to ~ 50 % in the presence of IN-GFP and ~ 30 % in the presence of IN-mCherry, further supporting this IN-DNA interaction. No clear band shifts were observed with LTR, however the intensity of the LTR band decreased to

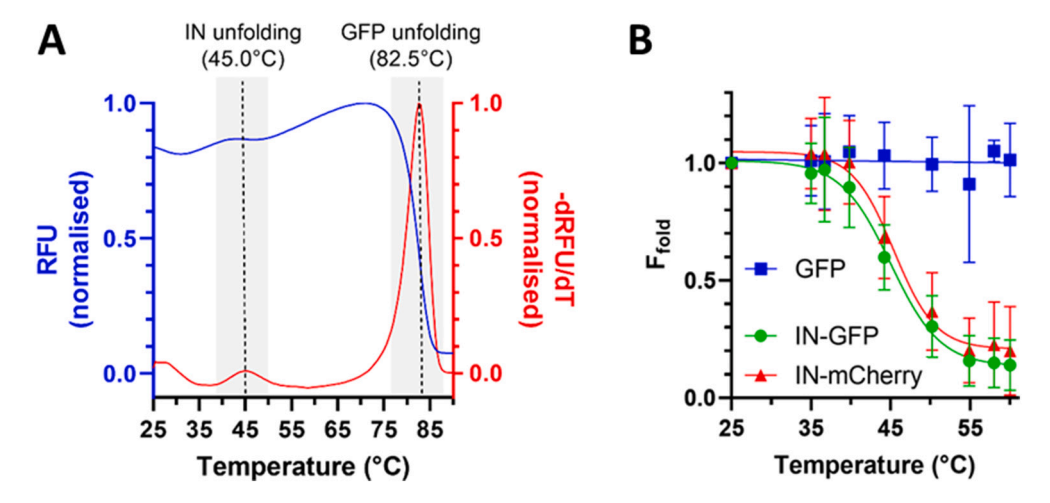


Fig. 1. Thermal stability of IN-GFP and IN-mCherry. A) DSF-GTP melt curve (normalised relative to the maximum measurement) for IN-GFP (CFX96 Touch Real-Time PCR set on the FAM channel). A T_m value of 45.0 °C was obtained for IN-GFP. B) T_{agg} values for IN-GFP and IN-mCherry were determined using FP-Basta (cf representative SDS-PAGE gel for IN-GFP and IN-mCherry in ESI Fig. 3). IN-GFP, IN-mCherry and GFP were combined, heated 10 min in a temperature gradient (25–60 °C), cooled 10 min, and centrifuged to remove aggregated protein. Buffer: phosphate buffer without RNAse treatment. Fluorescence was captured (GFP: blue light and 525 filter. mCherry: green light and 605 M filter). Band intensities were quantified (ImageJ) and normalised relative to 25 °C standards. Boltzmann sigmoidal regression was fitted for determination of T_{agg} values. Error bars represent SD (n = 4). RFU: relative fluorescence units. F_{fold} : fraction of folded protein.

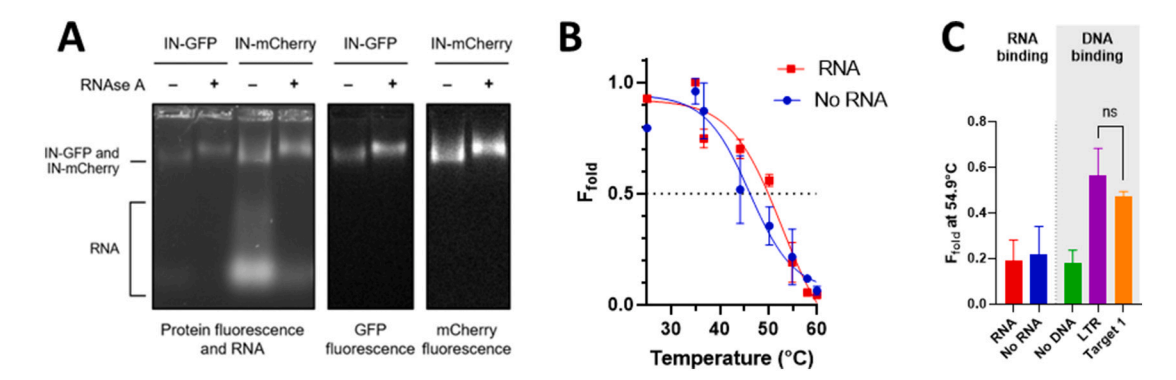


Fig. 2. Comparison of IN-GFP and IN-mCherry interactions with RNA and DNA. A) RNA present in IN-GFP and IN-mCherry samples before and after digestion with RNAse A (0.0055 Kunitz, 1 h, RT) was analysed via agarose gel electrophoresis (80 V, 40 min) in phosphate buffer. B) Thermal stability of RNA-contaminated IN-mCherry before and after digestion with RNAse A (0.0055 Kunitz, RT, 1 h). IN-mCherry was mixed with GFP and diluted in buffer IR (final protein concentrations = $10 \,\mu\text{M}$ each). Samples were heated in a temperature gradient (35–50 °C, 10 min), cooled on ice (10 min), and centrifuged (20 min). Fluorescence in the supernatant was measured in a black 96-well plate and normalised. Results were fitted with Boltzmann sigmoidal regression to determine T_{agg} values of 52.8 °C and 46.2 °C, before and after RNAse A digestion respectively. C) Isothermal FP-Basta reactions containing both IN-mCherry and GFP were performed with pLTR (7.5 μ M) or T1 (7.5 μ M) or buffer OA (54.9 °C, 10 min). Fluorescence of supernatant was measured as for B. Error bars represent SD (n = 2).

 ${\sim}65$ % with IN-GFP and ${\sim}40$ % with IN-mCherry (see ESI Fig. 4B), indicative of transient protein-DNA interactions.

3.4. qPCR-based strand transfer IN activity assay

We evaluated the suitability of our T1 and LTR design for the development of a user-friendly IN activity assay. Briefly, a pLTR or unprocessed LTR (uLTR) and T1 (see ESI Table 2) are combined with IN-GFP or IN-mCherry in the presence of 5 mM MnCl₂ and 5 mM MgCl₂ for 1 h. Integration products are then quantified by qPCR (Fig. 3A). Due to the non-site-specific nature of IN activity, LTRs can be randomly incorporated into either the top or bottom T1 strand. As such, two different primer sets are needed to capture these integration events. A universal LTR primer is used with either the T1 forward or reverse primer (see ESI Table 1) for qPCR amplification of bottom strand integration events or top strand integration events respectively. Of note, only integration events that occur downstream of the T1 primer binding site can be detected (see ESI Tables 4–5 for all detectable integration products).

An integration positive qPCR control template (see ESI Table 1) was

evaluated with two different qPCR premixes. Both premixes amplified the positive control with comparable primer efficiencies of 101.22 % and 98.99 % (see ESI Fig. 5A). Individual PCR amplification efficiency (see ESI Fig. 5B) was confirmed with LinRegPCR. Overall, amplification efficiency values were within the acceptable range [30], and the qPCR protocol did not require further optimisation. However, the BioRad iTaq $^{\rm TM}$ Universal SYBR® Green Supermix was more variable and abandoned (see ESI Fig. 5B).

The activity of IN-GFP and IN-mCherry was compared with reactions containing pLTR and T1. Comparable levels of integration products were detected (Fig. 3B). Control heat-treated IN-GFP and IN-mCherry, as well as GFP and mCherry samples yielded low background control levels of integration activity. Untreated IN-GFP and IN-mCherry results (n=4) were compared to pooled negative controls (n=12) confirming that the fusion proteins were similarly active (Fig. 3C). IN activity was then examined with uLTR (see ESI Table 2) to assess 3'-processing activity. IN-mCherry reactions performed with pLTR and uLTR yielded only slightly different mean Cq values of 23.7 ± 1.4 and 24.3 ± 0.9 respectively, suggesting that a 1-hour reaction at 37 °C was sufficient for the rate-limiting 3'-processing step and overall integration product yields to

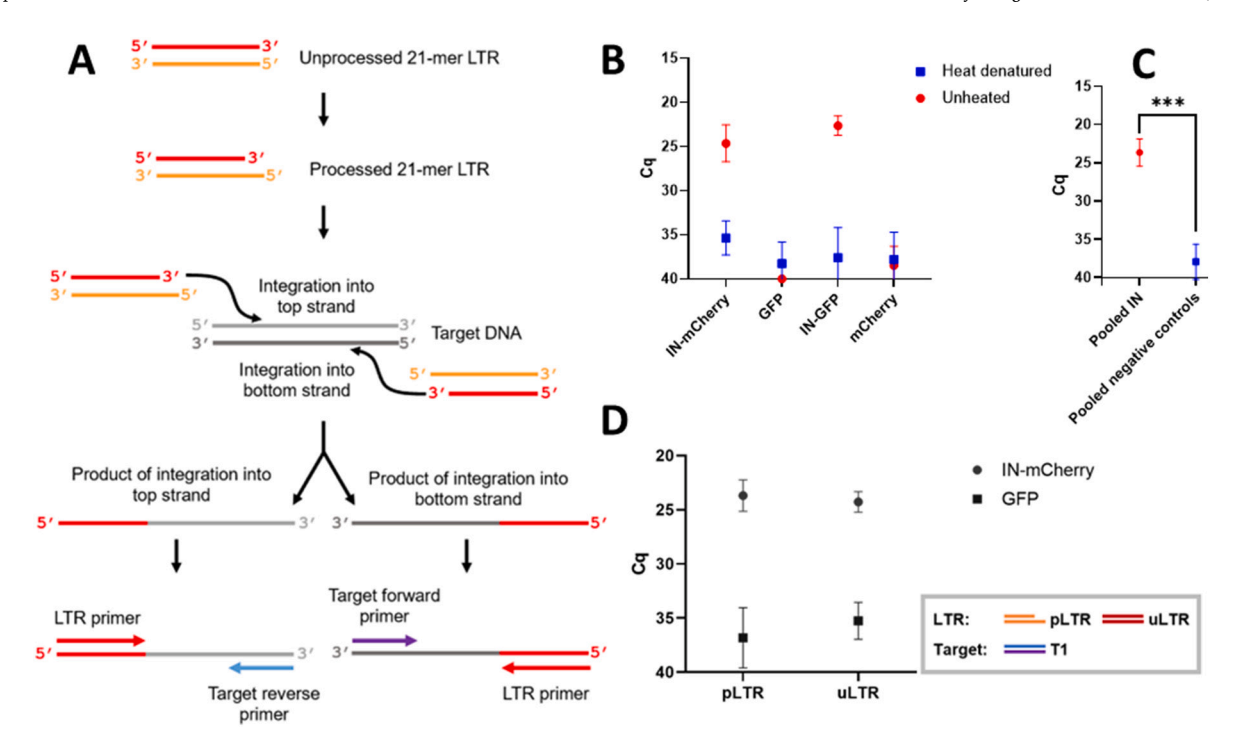


Fig. 3. A) Principle of the qPCR-based integrase activity assay. The viral LTR is processed and inserted into T1 DNA via IN strand transfer activity. Integration events are detected by qPCR. B) IN activity of IN-GFP and IN-mCherry. Negative background control reactions include GFP and mCherry, and heat-denatured (95 °C) IN-GFP or IN-mCherry. Cq values were obtained from amplification curves with a threshold set at 100 RFU (n = 2). A Cq value of 40 was assigned when no amplification was observed. C) Pooled Cq values for all active IN-GFP and IN-mCherry reactions (n = 4) and all negative background controls (n = 12). A Mann-Whitney test revealed a significant difference (p = 0.0005). D) IN activity with pLTR and uLTR. Reactions were run with T1 (37 °C for 1 h), followed by heat inactivation (90 °C for 10 min). IN reaction dilutions (1/200) were amplified (40-cycle qPCR protocol). Error bars represent SD (n = 3).

begin to plateau with the uLTR (Fig. 3D).

We examined T1 top strand and bottom strand integration products. Top and bottom strand qPCR data were similar (see ESI Fig. 6A). The amplified PCR product bands were further compared to the T1 by PAGE (see ESI Fig. 6B–C). IN-GFP and IN-mCherry integration reactions produce similar bands, while no band is visible in GFP and mCherry controls after 30 cycles. Theoretical $T_{\rm m}$ values were calculated for T1 and all

possible integration events (see ESI Tables 4–5) with Oligo Calculator version 3.27 [31]. Extensive $T_{\rm m}$ analyses confirmed that T1 was not amplified in the IN reactions (see ESI Figs. 6–7 and extended text 2). Comparatively, one additional integration event can occur in the T1 bottom strand. As such, the T1 forward primer was chosen for further qPCR assay evaluation.

Further reactions were performed to evaluate the limits of the assay.

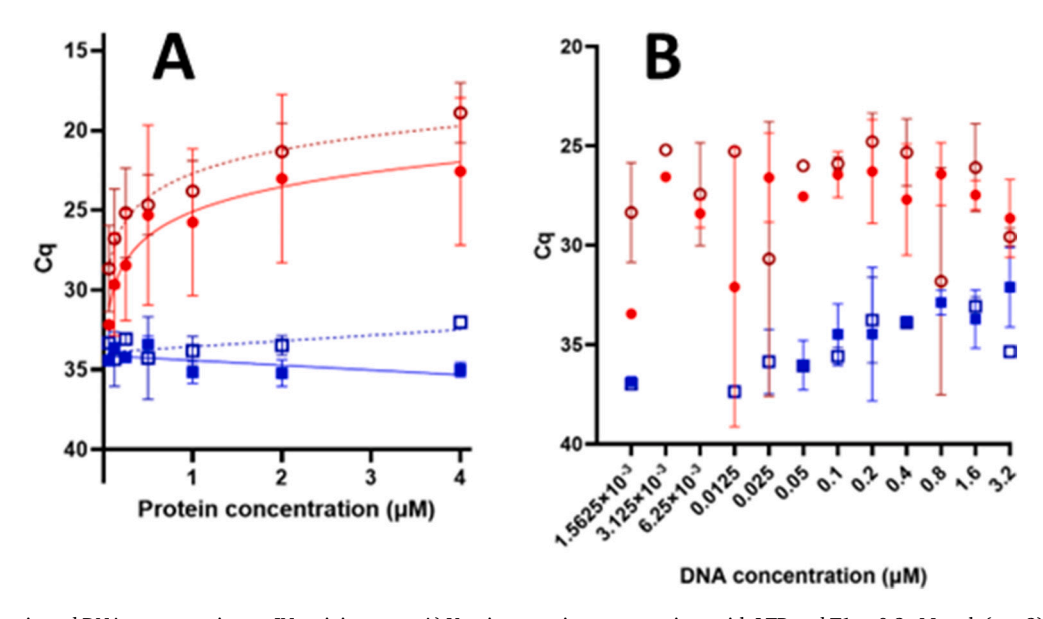


Fig. 4. Impact of protein and DNA concentration on IN activity assay. A) Varying protein concentrations with LTR and T1 at 0.2 μM each (n = 2). B) Varying LTR and T1 concentrations with protein at 1 μM (n = 2, except for 0.2 μM and 0.1 μM reactions n = 3). uLTR (solid symbol) and pLTR (open symbol) were systematically compared with IN-mCherry (red) or GFP control (blue) in buffer IR. Reactions were run at 37 °C for 1 h and inactivated at 90 °C for 10 min. All reactions were diluted (1/200) before qPCR. Error bars represent SD.

We first examined the impact of IN reaction dilutions and primer concentrations on qPCR. The data revealed that these parameters are relatively flexible and can be easily adapted (see ESI Fig. 8A–B and extended text 3). The IN reaction conditions such as protein and DNA concentrations were then examined. Initially, the activity of IN-mCherry

increased rapidly until its concentration reached $\sim 0.5~\mu M$ with both LTR species after which it started to plateau (Fig. 4A). However, at IN-mCherry concentrations $< 0.5~\mu M$ the difference in product yield was most significant between pLTR and uLTR reactions, consistent with the rate-limiting 3'-processing step [32]. In contrast, no significant change

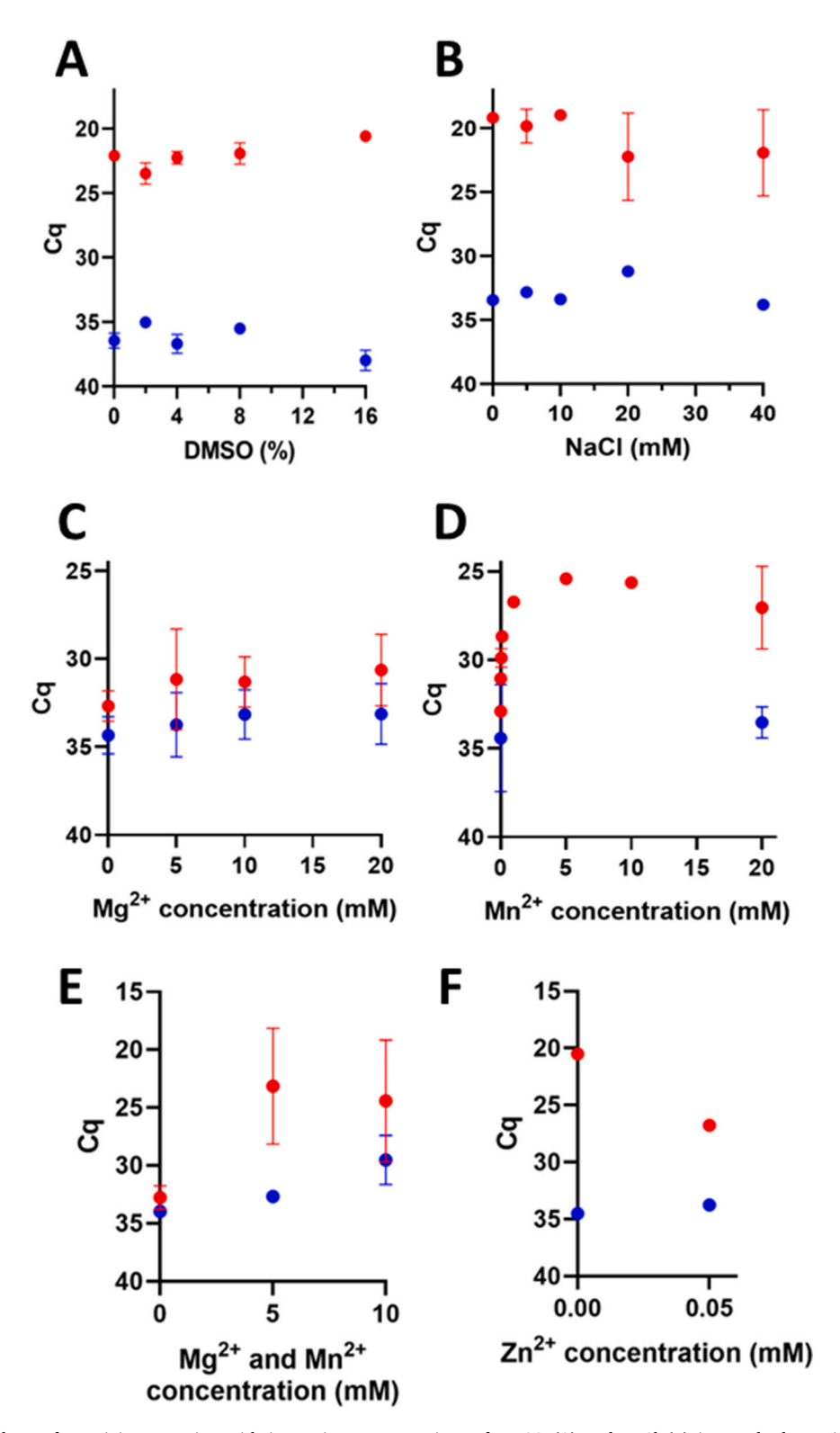


Fig. 5. IN-mCherry strand transfer activity screening with increasing concentrations of DMSO (A) and NaCl (B) in standard reactions conditions (buffer IR). Increasing concentrations of $MgCl_2$ (C), $MnCl_2$ (D), $MgCl_2$ and $MnCl_2$ (E) were compared. F) $Zn(CH_3CO_2)_2$ was assessed in standard reactions conditions (i.e. in the presence of 5 mM $MnCl_2$ and 5 mM $MgCl_2$). A-F) pLTR and T1 were used for all reactions. All reactions were run at 37 °C for 1 h and inactivated at 90 °C for 10 min. All reactions were diluted (1/200) before qPCR. IN-mCherry (red) and GFP control (blue). Error bars represent SD.

in background Cq values was observed with increasing GFP concentrations. When varying LTR and T1 concentrations were examined, no major impact was observed except for the lowest and highest concentrations. For these extreme conditions a significant reduction in activity was observed (Fig. 4B). Interestingly, Cq values progressively changed in the negative background GFP controls with increasing LTR and T1 concentrations possibly indicative of a small amount of DNA contaminants in the DNA stocks (Fig. 4B). Lastly, the temperature dependence of IN-mCherry activity was investigated (see ESI Fig. 9). The IN-mCherry activity was relatively stable (25–50 $^{\circ}$ C) with a somewhat expected maximal activity at 37.3 $^{\circ}$ C. Some minimal activity was observed at 4 $^{\circ}$ C indicating that reactions should be stored on ice to prevent IN activity during reaction setup.

3.5. Compound and metal ion screening

We examined the effect of common additives on IN-mCherry activity. Compounds are generally dissolved in DMSO for use in inhibitor screening campaigns. As such, increasing DMSO concentrations were examined in IN-mCherry reactions (Fig. 5A). A slight increase in IN activity was observed at the highest DMSO concentration which could be due to more efficient qPCR amplification, as DMSO is commonly used for PCR improvement [33,34]. IN is more soluble in higher salt conditions, however increasing NaCl can also reduce protein-DNA interactions [35]. As NaCl concentration increased, a slight decrease in integration products was observed (Fig. 5B), however, given error margins, no clear trend could be identified. The negative control background Cq values were mostly unaffected.

The divalent metal ion preference (i.e. Mg^{2+} or Mn^{2+}) of IN is dependent on reaction conditions [36]. As such our standard IN-mCherry reactions were set up with 5 mM Mg^{2+} and 5 mM Mn^{2+} . Here, we examined the IN activity with Mg^{2+} only, Mn^{2+} only, or a combination of Mg^{2+} and Mn^{2+} . IN activity was severely impacted in the presence of Mg^{2+} alone (Fig. 5C) which was further compounded by an increase in the negative control background products. In contrast, Integrase activity rose very quickly with increasing concentrations of Mn^{2+} with an obvious plateau reached at 5 mM followed by a downward trend at higher concentrations (Fig. 5D). IN was 54-fold more active in the presence of 5 mM Mn^{2+} than with 5 mM Mg^{2+} . A slightly higher IN activity was achieved with our standard 5 mM Mg^{2+} and Mn^{2+} conditions (Fig. 5E). However, higher concentrations of these metal ions were detrimental and increased background products. The data indicate that in our conditions, Mg^{2+} is not essential.

 Zn^{2+} has previously been reported to be required for IN tetramerization, and to increase Mg^{2+} -dependent IN activity [37]. However, Zn^{2+} has also been shown to cause aggregation of IN [13]. The IN activity reaction was supplemented with a low concentration of Zn^{2+} to determine whether Zn^{2+} could improve IN activity in the presence of Mg^{2+} and Mn^{2+} . However, addition of Zn^{2+} (50 μ M) resulted in a substantial inhibition of IN activity (Fig. 5F).

Increasing concentrations of EDTA were tested as an inhibitor in INmCherry reactions containing 5 mM Mn^{2+} and 5 mM Mg^{2+} . It should be noted that PCR efficiency was not affected even at the highest EDTA concentration used (e.g. maximum EDTA concentration in the qPCR is 40 μ M). As EDTA concentration increased, IN activity decreased (Fig. 6). The IN activity was completely abolished when EDTA was in excess relative to the combined divalent metal ion concentration.

3.6. Inter-assay reproducibility

The reproducibility of the IN assay was assessed by pooling and comparing Cq values from independent reactions using different IN-mCherry and GFP protein samples (Fig. 7). For this, reactions containing 1 μM of IN-mCherry or GFP, 0.2 μM T1 and 0.2 μM pLTR in buffer IR were selected. Overall, Cq values were normally distributed with mean Cq values of 23.21 \pm 2.491 for IN-mCherry reactions and 35.37 \pm 2.797

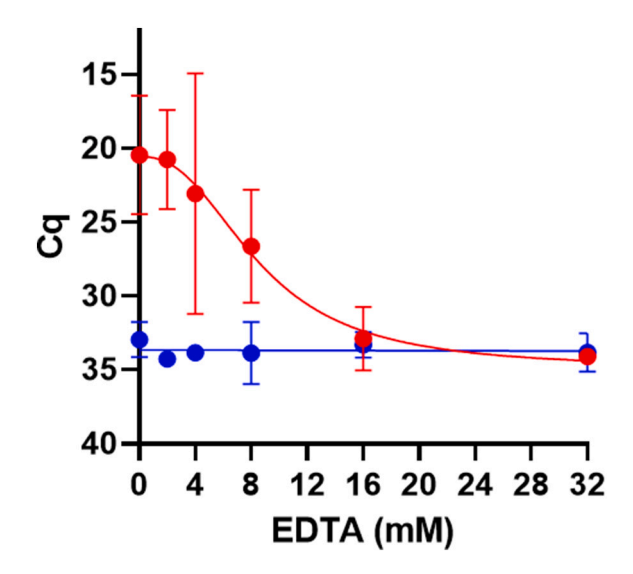


Fig. 6. Inhibition of IN-mCherry strand transfer activity. Reactions with pLTR, T1 and buffer IR and increasing EDTA were performed (37 $^{\circ}$ C, 1 h) followed by heat inactivation (90 $^{\circ}$ C, 10 min) in standard conditions. Reaction mixtures were then diluted and amplified using our standard qPCR protocol. GraphPad Prism 9.2.0 was used to fit IN-mCherry data (red) with sigmoidal regression, while GFP data (blue) was fitted with simple linear regression. Error bars represent SD (n = 2).

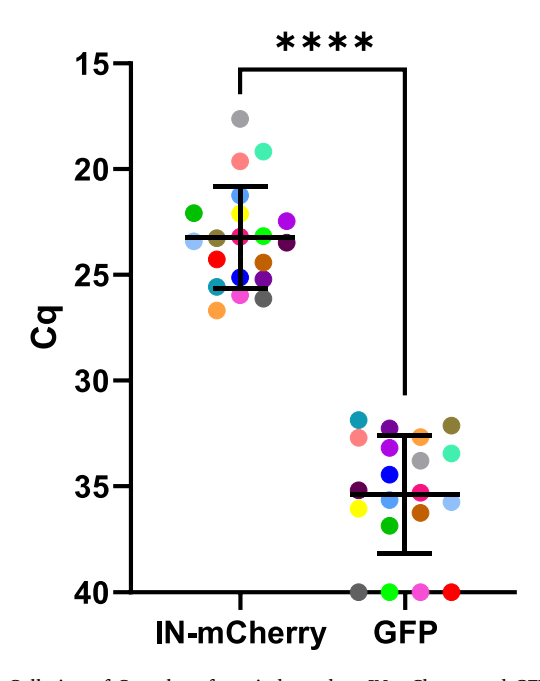


Fig. 7. Collation of Cq values from independent IN-mCherry and GFP strand transfer reactions. IN-mCherry and their associated GFP control reactions are shown in the same colour. All reactions included 1 μ M protein, 0.2 μ M pLTR DNA and 0.2 μ M T1 in buffer IR. Statistical analysis in GraphPad Prism 9.2.0 was performed, utilising a D'Agostino and Pearson normality test (ns) followed by an unpaired t-test (p < 0.0001). Error bars represent SD (n = 20).

for GFP. It is likely that varying protein aggregation in IN-mCherry and GFP samples is causing the dispersion of Cq values (Fig. 7). To avoid this, comparable reactions should be performed simultaneously with the same reagents. Overall, the IN-mCherry activity assay is robust yielding reliable data with a satisfactory level of separation even when comparing independent repeats performed with different protein and DNA samples, buffers, and reagents.

4. Discussion

4.1. IN-GFP and IN-mCherry are versatile tools for FP-EMSA and FP-

Wild-type IN has low solubility, making it difficult to produce and purify [16]. Despite higher yields of soluble IN-mCherry, the final yields of IN-mCherry and IN-GFP were both very low. Neither IN-mCherry nor IN-GFP were binding effectively to the nickel affinity resin. The structure of IN-mCherry was modelled using AlphaFold Colab [38] (see ESI Fig. 10) and suggested that shielding of the His6 tag within the fusion protein was unlikely. RNA and DNA contaminants bound to IN [5] are more likely hindering nickel resin binding. Higher salt conditions could be trialled for future purifications to minimise interactions between DNA or RNA and IN. While low yields were not ideal, the purified INmCherry and IN-GFP proteins were correctly folded and functional. Our T_{m} and T_{agg} values were lower than previously reported literature values [27,28]. Differences were attributed to buffer differences and ramp speed [39]. Interestingly, stable oligomeric fluorescent IN bands were observed in SDS gels (see ESI Fig. 3). Gel filtration may be used to separate oligomeric IN to investigate their impact on thermal stability and activity. The FP-EMSA and FP-Basta clearly showed that IN-GFP and IN-mCherry interacted with DNA. Moreover, the DNA binding activity of IN-GFP and IN-mCherry was comparable. Overall, FP-EMSA and FP-Basta have potential to be used as secondary assays to assess the various functions and properties of these fluorescent IN in the presence of other proteins. For example, the FP-Basta could be very advantageous for confirmation of direct protein binding by an inhibitor in crude samples.

4.2. A robust and user-friendly strand transfer IN assay

The new qPCR IN assay enables sensitive detection of DNA integration products from the strand transfer activity of IN-mCherry and IN-GFP. Under the standard assay conditions, a significant number of integration events could be detected (i.e. ~21,500 times more than the background) highlighting the utility of the assay. Examination of amplified integration products revealed several discrete DNA bands (see ESI Fig. 6B–C). IN-GFP and IN-mCherry both seemed to prefer certain sites for integration within the T1. IN has previously been shown to have some target sequence preference [40–42]. The simplicity of our assay offers opportunities to explore other DNA sequences and secondary structures for inclusion in this new assay.

High NaCl concentrations improve the stability and solubility of IN but impair its binding to DNA [35]. Several IN activity assays include low concentrations of NaCl, possibly improving IN solubility [28,43,44]. NaCl concentrations up to 40 mM had no substantial impact on INmCherry activity suggesting that high concentrations of NaCl could be incorporated into concentrated IN-mCherry stocks for improved stability in long-term storage conditions. Formation of insoluble aggregates may impact the IN-mCherry-catalysed integration reactions, possibly reducing the level of agreement between independent reactions performed at different times (Fig. 7). A mutant IN with better solubility [16] may be an option to limit these issues. Furthermore, storing IN-mCherry in single-use aliquots to reduce freeze-thaw cycles, along with a high salt storage buffer, may improve inter-assay reproducibility.

IN activity assays generally require an IN concentration 2- to 10-fold higher than DNA [28,43–45]. The 3'-processing and strand transfer activities increased with IN-mCherry concentration up to a 20-fold excess of protein over DNA (Fig. 4A). However, assay conditions were adequate at a 5-fold excess of IN-mCherry. DNA concentration had minimal impact on product yields, and background noise was reduced by lowering LTR concentration. IN activity assays are generally performed at 37 $^{\circ}$ C [28,43–45]. While our reactions at 37 $^{\circ}$ C were optimal, room temperature was also effective. Overall, reaction conditions appeared to be flexible, indicating that reagent concentrations and temperature can

be adapted to suit the application of the in vitro assay.

4.3. Mn^{2+} is essential for the IN activity assay

IN activity assays have been performed with Mg²⁺ [28,43,44], Mn²⁺ [45,46], or a combination of both [47]. Preference of metal ion by IN depends on the reaction conditions [36]. While Mg²⁺ is more biologically relevant due to its high physiological concentration, Mg²⁺dependent IN activity is more sensitive to the viral DNA sequence [32]. In contrast, Mn²⁺-dependent IN activity is more tolerant of sequence variation [32]. In our assay conditions, the IN activity was highly dependent on Mn²⁺ (Fig. 5D). Of note, 5 mM Mn²⁺ yielded 56-fold more IN activity than 5 mM Mg²⁺. As Zn²⁺ in combination with Mg²⁺ promotes IN self-association [37], we hypothesised that it could increase IN activity. However, our results showed that 50 μM Zn²⁺ decreased INmCherry activity 79-fold in the presence of Mg^{2+} and Mn^{2+} (Fig. 5F). It is possible that IN-mCherry may have associated with Zn^{2+} during protein expression, and further addition of Zn²⁺ may have triggered protein aggregation. Notably, the Zn²⁺ concentration in our experiment were 50-fold higher in molar excess over IN representing a clear limitation. While Zn²⁺-induced protein aggregation has been observed with IN-GFP previously [13], drawing conclusions from our single experiment would be premature. Overall, Zn²⁺ did not appear to contribute to IN activity, and Mn^{2+} was clearly the preferred co-factor in our assay conditions.

4.4. Conclusions and perspective

IN assays generally require a minimum incubation time of 1 h, and up to 18 h [28,43-45,47]. The qPCR IN activity assay can be performed in \sim 2 h with a minimal number of steps or special requirements compared with other assays [28,43-45,47] (see ESI Table 6) and was validated for inhibitor screening with EDTA. Full inhibition of INmCherry could be achieved with a clear 'yes or no' result. The qPCR IN activity assay has potential applications for structure-activity relationship studies and to distinguish whether a compound inhibits 3'processing or strand transfer activity. IN-mCherry and IN-GFP are fully functional with no major differences in their activity and can be used interchangeably in our assays. The FP-Basta could be applied to examine direct ligand binding to IN. Of note, EDTA or classic INSTI do not affect the thermal stability of IN [28] as they chelate Mg²⁺ or Mn²⁺ ions. As such, experimental compounds such as noncatalytic site integrase inhibitors [28,48] could be trialled to further validate the FP-Basta. Overall, the FP-Basta and qPCR IN activity assay leveraging our fluorescent IN offer a comprehensive suite of user-friendly assays capable of interrogating all IN functions with potential to fast track HIV drug discovery. Finally, the simplicity and low-cost of these new assays should facilitate their adoption and translation into a high-throughput screening platform.

CRediT authorship contribution statement

Rebecca A. Bourquin: Writing – original draft, Validation, Methodology, Investigation, Formal analysis, Data curation. Alanna E. Sorenson: Writing – review & editing, Validation, Supervision, Methodology. Patrick M. Schaeffer: Writing – review & editing, Writing – original draft, Validation, Supervision, Project administration, Methodology, Conceptualization.

Declaration of competing interest

The authors declare that they have no known competing financial interests or personal relationships that could have appeared to influence the work reported in this paper.

Appendix A. Supplementary data

Supplementary data to this article can be found online at https://doi.org/10.1016/j.jjbiomac.2025.142859.

Data availability

Data will be made available on request.

References

- [1] World Health Organisation, HIV/AIDS Fact Sheet, 2021.
- [2] World Health Organisation, in: H.a.S.P. Global HIV (Ed.), Latest HIV Estimates and Updates on HIV Policies Uptake, December 2021, 2021.
- [3] A.V. Zhao, R.D. Crutchley, R.C. Guduru, K. Ton, T. Lam, A.C. Min, A clinical review of HIV integrase strand transfer inhibitors (INSTIs) for the prevention and treatment of HIV-1 infection, Retrovirology 19 (1) (2022) 22.
- [4] F. Shalbi, A.R. Ali, A mini-review on integrase inhibitors: the cornerstone of next-generation HIV treatment, Eur. J. Med. Chem. 279 (2024) 116900.
- [5] J.J. Kessl, S.B. Kutluay, D. Townsend, S. Rebensburg, A. Slaughter, R.C. Larue, N. Shkriabai, N. Bakouche, J.R. Fuchs, P.D. Bieniasz, M. Kvaratskhelia, HIV-1 integrase binds the viral RNA genome and is essential during Virion morphogenesis, Cell 166 (5) (2016) 1257–1268.e12.
- [6] A. Engelman, F.D. Bushman, R. Craigie, Identification of discrete functional domains of HIV-1 integrase and their organization within an active multimeric complex, EMBO J. 12 (8) (1993) 3269–3275.
- [7] Y. Goldgur, F. Dyda, A.B. Hickman, T.M. Jenkins, R. Craigie, D.R. Davies, Three new structures of the core domain of HIV-1 integrase: an active site that binds magnesium, Proc. Natl. Acad. Sci. U. S. A. 95 (16) (1998) 9150–9154.
- [8] P.A. Sherman, J.A. Fyfe, Human immunodeficiency virus integration protein expressed in Escherichia coli possesses selective DNA cleaving activity, Proc. Natl. Acad. Sci. U. S. A. 87 (13) (1990) 5119–5123.
- [9] C. Vink, A. Groeneger, R.H.A. Plasterk, Identification of the catalytic and DNAbinding region of the human-immunodeficiency-virus type-I integrase protein, Nucleic Acids Res. 21 (6) (1993) 1419–1425.
- [10] A. Engelman, K. Mizuuchi, R. Craigie, HIV-1 DNA integration: mechanism of viral DNA cleavage and DNA strand transfer, Cell 67 (6) (1991) 1211–1221.
- [11] K. Anstett, B. Brenner, T. Mesplede, M.A. Wainberg, HIV drug resistance against strand transfer integrase inhibitors, Retrovirology 14 (1) (2017) 36.
- [12] P.S. Mahajan, S.J. Smith, M. Li, R. Craigie, S.H. Hughes, X.Z. Zhao, T.R. Burke Jr., N-substituted bicyclic carbamoyl Pyridones: integrase Strand transfer inhibitors that potently inhibit drug-resistant HIV-1 integrase mutants, ACS Infect Dis 10 (3) (2024) 917–927.
- [13] A.E. Sorenson, P.M. Schaeffer, A new bivalent fluorescent fusion protein for differential cu(II) and Zn(II) ion detection in aqueous solution, Anal. Chim. Acta 1101 (2020) 120–128.
- [14] D. Schenkwein, V. Turkki, H.R. Karkkainen, K. Airenne, S. Yla-Herttuala, Production of HIV-1 integrase fusion protein-carrying lentiviral vectors for gene therapy and protein transduction, Hum. Gene Ther. 21 (5) (2010) 589–602.
- [15] L. Mestrom, S. Marsden, M. Dieters, P. Achterberg, L. Stolk, I. Bento, U. Hanefeld, P. Hagedoorn, Artificial fusion of mCherry enhanced solubility and stability of Trehalose transferase, Appl. Environ. Microbiol. 85 (8) (2019).
- [16] T.M. Jenkins, A. Engelman, R. Ghirlando, R. Craigie, A soluble active mutant of HIV-1 integrase: INVOLVEMENT OF BOTH THE CORE AND CARBOXYL-TERMINAL DOMAINS IN MULTIMERIZATION (*), J. Biol. Chem. 271 (13) (1996) 7712–7718.
- [17] G. Eilers, K. Gupta, A. Allen, J. Zhou, Y. Hwang, M.B. Cory, F.D. Bushman, G. Van Duyne, Influence of the amino-terminal sequence on the structure and function of HIV integrase, Retrovirology 17 (1) (2020) 28.
- [18] M. Li, R. Yang, X. Chen, H. Wang, R. Ghirlando, E.K. Dimitriadis, R. Craigie, HIV-1 integrase assembles multiple species of stable synaptic complex Intasomes that are active for concerted DNA integration in vitro, J. Mol. Biol. 436 (10) (2024) 168557.
- [19] M. Moreau, I. Morin, P. Schaeffer, Quantitative determination of protein stability and ligand binding using a green fluorescent protein reporter system, Mol. Biosyst. 6 (2010) 1285–1292.
- [20] M.J.J. Moreau, I. Morin, S.P. Askin, A. Cooper, N.J. Moreland, S.G. Vasudevan, P. M. Schaeffer, Rapid determination of protein stability and ligand binding by differential scanning fluorimetry of GFP-tagged proteins, RSC Adv. 2 (31) (2012) 11892–11900.
- [21] A.E. Sorenson, P.M. Schaeffer, Electrophoretic mobility shift assays with GFP-tagged proteins (GFP-EMSA), Methods Mol. Biol. 2089 (2020) 159–166.
- [22] M.S. Rana, X. Wang, A. Banerjee, An improved strategy for fluorescent tagging of membrane proteins for overexpression and purification in mammalian cells, Biochemistry 57 (49) (2018) 6741–6751.
- [23] F.H. Niesen, H. Berglund, M. Vedadi, The use of differential scanning fluorimetry to detect ligand interactions that promote protein stability, Nat. Protoc. 2 (9) (2007) 2212–2221
- [24] M.W. Pantoliano, E.C. Petrella, J.D. Kwasnoski, V.S. Lobanov, J. Myslik, E. Graf, T. Carver, E. Asel, B.A. Springer, P. Lane, F.R. Salemme, High-density miniaturized thermal shift assays as a general strategy for drug discovery*, SLAS Discovery 6 (6) (2001) 429–440.

- [25] M.-C. Lo, A. Aulabaugh, G. Jin, R. Cowling, J. Bard, M. Malamas, G. Ellestad, Evaluation of fluorescence-based thermal shift assays for hit identification in drug discovery, Anal. Biochem. 332 (1) (2004) 153–159.
- [26] G.V. Semisotnov, N.A. Rodionova, O.I. Razgulyaev, V.N. Uversky, A.F. Gripas, R. I. Gilmanshin, Study of the "molten globule" intermediate state in protein folding by a hydrophobic fluorescent probe, Biopolymers 31 (1) (1991) 119–128.
- [27] F. Christ, S. Shaw, J. Demeulemeester, B.A. Desimmie, A. Marchand, S. Butler, W. Smets, P. Chaltin, M. Westby, Z. Debyser, C. Pickford, Small-molecule inhibitors of the LEDGF/p75 binding site of integrase block HIV replication and modulate integrase multimerization, Antimicrob. Agents Chemother. 56 (8) (2012) 4365–4374.
- [28] J.J. Kessl, N. Jena, Y. Koh, H. Taskent-Sezgin, A. Slaughter, L. Feng, S. de Silva, L. Wu, S.F. Le Grice, A. Engelman, J.R. Fuchs, M. Kvaratskhelia, Multimode, cooperative mechanism of action of allosteric HIV-1 integrase inhibitors, J. Biol. Chem. 287 (20) (2012) 16801–16811.
- [29] A.E. Sorenson, P.M. Schaeffer, Real-time temperature sensing using a Ratiometric dual fluorescent protein biosensor, Biosensors (Basel) 13 (3) (2023).
- [30] G. Johnson, T. Nolan, S.A. Bustin, Real-time quantitative PCR, pathogen detection and MIQE, in: M. Wilks (Ed.), PCR Detection of Microbial Pathogens, Humana Press, Totowa, NJ, 2013, pp. 1–16.
- [31] W.A. Kibbe, OligoCalc: an online oligonucleotide properties calculator, Nucl. Acids Res. 35 (Web Server issue) (2007) W43–W46.
- [32] O. Delelis, K. Carayon, A. Saib, E. Deprez, J.F. Mouscadet, Integrase and integration: biochemical activities of HIV-1 integrase, Retrovirology 5 (2008) 114.
- [33] P.R. Winship, An improved method for directly sequencing PCR amplified material using dimethyl sulphoxide, Nucleic Acids Res. 17 (3) (1989) 1266.
- [34] R. Chakrabarti, C.E. Schutt, The enhancement of PCR amplification by low molecular-weight sulfones, Gene 274 (1–2) (2001) 293–298.
- [35] I.R. Haugan, B.M. Nilsen, S. Worland, L. Olsen, D.E. Helland, Characterization of the DNA-binding activity of HIV-1 integrase using a filter binding assay, Biochem. Biophys. Res. Commun. 217 (3) (1995) 802–810.
- [36] A. Engelman, R. Craigie, Efficient magnesium-dependent human immunodeficiency virus type 1 integrase activity, J. Virol. 69 (9) (1995) 5908–5911.
- [37] S.P. Lee, J. Xiao, J.R. Knutson, M.S. Lewis, M.K. Han, Zn2+ promotes the self-association of human immunodeficiency virus type-1 integrase in vitro, Biochemistry 36 (1) (1997) 173–180.
- [38] J. Jumper, R. Evans, A. Pritzel, T. Green, M. Figurnov, O. Ronneberger, K. Tunyasuvunakool, R. Bates, A. Žídek, A. Potapenko, A. Bridgland, C. Meyer, S.A. A. Kohl, A.J. Ballard, A. Cowie, B. Romera-Paredes, S. Nikolov, R. Jain, J. Adler, T. Back, S. Petersen, D. Reiman, E. Clancy, M. Zielinski, M. Steinegger, M. Pacholska, T. Berghammer, S. Bodenstein, D. Silver, O. Vinyals, A.W. Senior, K. Kavukcuoglu, P. Kohli, D. Hassabis, Highly accurate protein structure prediction with AlphaFold, Nature 596 (7873) (2021) 583–589.
- [39] S.O. Ugwu, S.P. Apte, The effect of buffers on protein conformational stability, Pharm. Technol. 28 (2004) 86–108.
- [40] D. Michieletto, M. Lusic, D. Marenduzzo, E. Orlandini, Physical principles of retroviral integration in the human genome, Nat. Commun. 10 (1) (2019) 575.
- [41] E. Serrao, L. Krishnan, M.-C. Shun, X. Li, P. Cherepanov, A. Engelman, G. N. Maertens, Integrase residues that determine nucleotide preferences at sites of HIV-1 integration: implications for the mechanism of target DNA binding, Nucleic Acids Res. 42 (8) (2014) 5164–5176.
- [42] A.G. Holman, J.M. Coffin, Symmetrical base preferences surrounding HIV-1, avian sarcoma/leukosis virus, and murine leukemia virus integration sites, Proc. Natl. Acad. Sci. 102 (17) (2005) 6103–6107.
- [43] H. Yan, T.C. Mizutani, N. Nomura, T. Takakura, Y. Kitamura, H. Miura, M. Nishizawa, M. Tatsumi, N. Yamamoto, W. Sugiura, A novel small molecular weight compound with a carbazole structure that demonstrates potent human immunodeficiency virus type-1 integrase inhibitory activity, Antivir. Chem. Chemother. 16 (6) (2005) 363–373.
- [44] A. Pflieger, P. Waffo Teguo, Y. Papastamoulis, S. Chaignepain, F. Subra, S. Munir, O. Delelis, P. Lesbats, C. Calmels, M.L. Andreola, J.M. Merillon, C. Auge-Gouillou, V. Parissi, Natural stilbenoids isolated from grapevine exhibiting inhibitory effects against HIV-1 integrase and eukaryote MOS1 transposase in vitro activities, PloS One 8 (11) (2013) e81184.
- [45] Y. Wang, H. Klock, H. Yin, K. Wolff, K. Bieza, K. Niswonger, J. Matzen, D. Gunderson, J. Hale, S. Lesley, K. Kuhen, J. Caldwell, A. Brinker, Homogeneous high-throughput screening assays for HIV-1 integrase 3beta-processing and strand transfer activities, J. Biomol. Screen. 10 (5) (2005) 456–462.
- [46] Y. Wang, H.Q. Lin, P. Wang, J.S. Hu, T.M. Ip, L.M. Yang, Y.T. Zheng, D. Chi-Cheong Wan, Discovery of a novel HIV-1 integrase/p75 interacting inhibitor by docking screening, biochemical assay, and in vitro studies, J. Chem. Inf. Model. 57 (9) (2017) 2336–2343.
- [47] S. Abrahams, S. Mosebi, M.Q. Fish, M.A. Papathanasopoulos, R. Hewer, Screening of the NIH clinical collection for inhibitors of HIV-1 integrase activity, S. Afr. J. Sci. 114 (3–4) (2018).
- [48] L.D. Fader, E. Malenfant, M. Parisien, R. Carson, F. Bilodeau, S. Landry, M. Pesant, C. Brochu, S. Morin, C. Chabot, T. Halmos, Y. Bousquet, M.D. Bailey, S.H. Kawai, R. Coulombe, S. LaPlante, A. Jakalian, P.K. Bhardwaj, D. Wernic, P. Schroeder, M. Amad, P. Edwards, M. Garneau, J. Duan, M. Cordingley, R. Bethell, S.W. Mason, M. Bos, P. Bonneau, M.A. Poupart, A.M. Faucher, B. Simoneau, C. Fenwick, C. Yoakim, Y. Tsantrizos, Discovery of BI 224436, a noncatalytic site integrase inhibitor (NCINI) of HIV-1, ACS Med. Chem. Lett. 5 (4) (2014) 422–427.